JGR Oceans

RESEARCH ARTICLE
10.1029/2020JC016978

Key Points:

- An expression for the turbulent kinetic energy of turbulence is formulated in terms of readily measured properties
- The vertical variation of the turbulent length scale is found to be important
- There are implications for the vertical variation of the turbulent eddy diffusivity

Correspondence to:
K. J. Richards,
rkelvin@hawaii.edu

Citation:
Richards, K. J., Natarov, A., & Carter, G. S. (2021). Scaling of shear-generated turbulence: The equatorial thermocline, a case study. *Journal of Geophysical Research: Oceans*, *126*, e2020JC016978. https://doi.org/10.1029/2020JC016978

Received 12 NOV 2020
Accepted 21 APR 2021

Scaling of Shear-Generated Turbulence: The Equatorial Thermocline, a Case Study

K. J. Richards[1,2], A. Natarov[1], and G. S. Carter[2]

[1]International Pacific Research Center, University of Hawai'i at Mānoa, Honolulu, HI, USA, [2]Department of Oceanography, University of Hawai'i at Mānoa, Honolulu, HI, USA

Abstract We formulate an expression for the turbulent kinetic energy dissipation rate, ϵ, associated with shear-generated turbulence in terms of quantities in the ocean or atmosphere that, depending on the situation, may be measurable or resolved in models. The expression depends on the turbulent vertical length scale, ℓ_v, the inverse time scale N, and the Richardson number $Ri = N^2/S^2$, where S is the vertical shear, with ℓ_v scaled in a way consistent with theories and observations of stratified turbulence. Unlike previous studies, the focus is not so much on the functional form of Ri, but the vertical variation of the length scale ℓ_v. Using data from two ~7-day time series in the western equatorial Pacific, the scaling is compared with the observed ϵ. The scaling works well with the estimated ϵ capturing the differences in amplitude and vertical distribution of the observed ϵ between the two times series. Much of those differences are attributable to changes in the vertical distribution of the length scale ℓ_v, and in particular the associated turbulent velocity scale, u_t. We relate u_t to a measure of the fine-scale variations in velocity, $\tilde{u}$. Our study highlights the need to consider the length scale and its estimation in environmental flows. The implications for the vertical variation of the associated turbulent diffusivity are discussed.

Plain Language Summary Turbulence generated by sheared motions can have a large impact on the mixing of properties in both the ocean and atmosphere. There is a need to elucidate the factors controlling the level of turbulence and in particular its vertical distribution. Here, we formulate an expression for the turbulence and test it against measurements taken in the western equatorial Pacific. We find a good correspondence highlighting the need to take into account the vertical variation of small-scale flow features. The results will be useful in interpreting observations and accounting for the turbulence in numerical models.

1. Introduction

Shear-generated turbulence in stably stratified environmental flows often makes an important contribution to the vertical transport of properties. Because of this, there have been numerous studies to develop parameterization schemes that provide an estimate of these turbulent fluxes with varying degrees of sophistication. Here, we consider the scaling of the turbulent kinetic dissipation rate, ϵ, a measure of turbulent activity. The scaling is put in terms of readily measured properties of the flow or easily derived quantities in models. As such the scaling can form the basis of a parameterization scheme to estimate turbulent fluxes from observations and be included in models of the ocean and atmosphere.

A large number of schemes relate the turbulent activity to the local gradient Richardson number, $Ri = N^2/S^2$, where N and S are the buoyancy frequency and vertical shear, respectively. In doing so, it is important that both N and the turbulence generating shear S are adequately resolved, something which is not always the case in the application of such schemes (cf., Richards et al., 2015). Much of the focus has been on the functional form of the Richardson number; see for example, Pacanowski and Philander (1981), Peters et al. (1988), and Figure 1 of Zaron and Moum (2009). As pointed out by Zaron and Moum (2009), however, the turbulent properties also depend on an appropriate length and time scale. Our focus will be on the turbulent vertical length scale, ℓ_v, its vertical variation and its impact on the vertical variation of the turbulent kinetic energy dissipation rate, ϵ, and associated vertical diffusion coefficient, κ_v.

In this study we formulate an expression for ϵ that depends on the length scale, ℓ_v, the inverse time scale N, and the Richardson number Ri. Using a similar expression, and observations from the western equatorial Pacific with both S and N well resolved, Richards et al. (2015) find that the implied length scale ℓ_v is

consistent with studies on stratified turbulence. We extend their work by consideration of the vertical variation of ℓ_v, and in particular the associated turbulent velocity scale, u_t. The scaling is compared to additional measurements of ϵ in the western equatorial Pacific. The comparison is very encouraging and highlights the importance of the vertical variation of the turbulent velocity scale.

2. Data and Physical Setting

Data were collected from cruise KM1208 of the R/V Kilo Moana to the western equatorial Pacific in April/May 2012. Here, we consider data taken on a meridional transect along 156°E from 5°N to 1°S, during April 20–24, with stations at half degree intervals together with two time series. The two time series were conducted at the equator (nominally) and 1.375 N, 156°E, for 8 and 7 days, respectively. For the first 3 days of the equatorial time series, the ship performed a butterfly pattern of side half a degree (∼50 km). The variation of properties on this scale was found to be small so the remainder of the time series was conducted from a stationary ship at the equator.

The combination of instruments used was similar to that described in Richards et al. (2015) with the exception that an untethered microstructure probe was used. High vertical resolution velocity data were collected using a 600-kHz Teledyne RDI Workhorse Acoustic Doppler Current Profiler attached to a CTD frame and operated in lowered mode (LADCP). CTD/LADCP profiles were taken at a nominal 2 h interval to a depth of 500 m during the two time series. A total of 89 CTD/LADCP profiles were taken during each time series. Turbulence measurements were taken during the two time series using a (untethered) Rockland VMP 6000 fitted with two shear probes and two rapid temperature probes (FP07). Noise induced by vibrations was removed using the Goodman algorithm (Goodman et al., 2006) and ϵ was averaged between the two shear probes. The average fall speed was 0.55 m s^{-1}. A total of 24 and 26 VMP profiles were taken during the equatorial and 1.375°N time series, respectively, at irregular intervals but spanning the duration of each time series. All VMP profiles were deeper than 500 m with most being full depth (∼1,940 and ∼2,400 m at the two sites, respectively).

The LADCP and VMP data were processed in the same way as described in Richards et al. (2015). In particular, the LADCP velocity data were binned at 2 m depth intervals. The turbulent kinetic energy dissipation rate, ϵ, calculated from the microstructure shear measurements, was also averaged over 2 m with overlapping bins (giving a value every 1 m). As shown by Richards et al. (2015), the relatively high vertical resolution, particularly the LADCP velocity, is needed to capture the fine-scale flow features that generate the turbulence.

The eastward (zonal) component of velocity, u, along the meridional section is shown in Figure 1a. Also plotted are contours of potential density and the mixed layer depth. The latter is determined as the depth at which the potential density first exceeds the surface density by $\Delta\sigma = 0.02$ kg m^{-3} (a value that captures well the depth to which surface induced turbulence penetrates). The mixed layer depth is in general shallower than 50 m except toward the northern extreme of the section.

At this time and longitude, the equatorial undercurrent (EUC) is centered at a depth of around 220 m and displaced south of the equator. The north equatorial counter current (NECC) is centered at 2.5°N and 120 m depth. At the surface close to the equator, the eastward flowing current is a result of a westerly wind event that occurred just prior to the section being made.

The vertical shear of the meridional component of velocity, $\partial v/\partial z$, and buoyancy frequency, N, are shown in Figure 2 for the two time series. (The few cases of $N^2 < 0$ are set to zero.) The quantities are plotted on potential density surfaces mapped back to the mean depth of each surface. Both quantities are seen to have features that have a relatively small vertical scale (SVS) that are persistent in time (particularly at the equator). We will refer to such features as SVS features. The SVS features have a somewhat different character at the equator and 1.375°N. At the equator, the higher amplitude SVS features are distributed between 100 and 250 m depth, while at 1.375°N they are concentrated around 175 m.

The variance preserving spectra of the zonal and meridional components of vertical shear, $\partial u/\partial z$ and $\partial v/\partial z$, respectively, where z is the vertical coordinate (Figure 3), have peaks at around 25–40 m wavelength. The spectra are calculated from profiles between 75 and 250 m depth. It is noteworthy that the peak in the shear

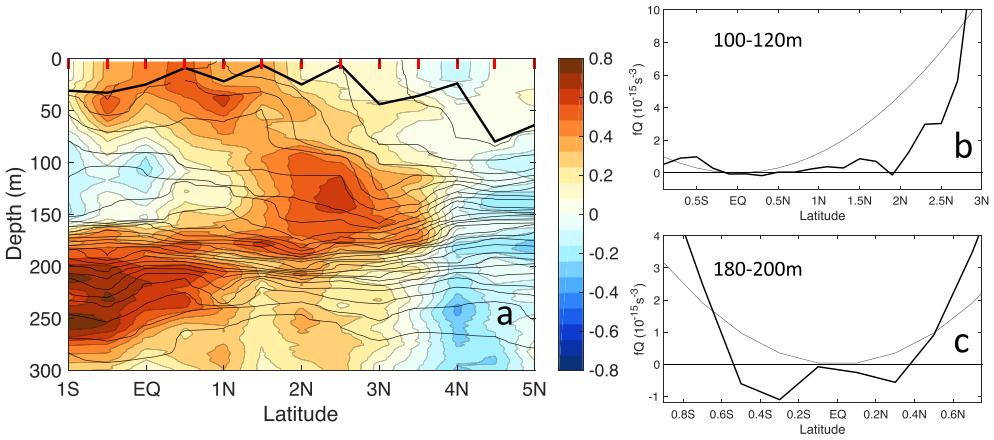

Figure 1. (a) The eastward (zonal) component of velocity, u, measured along 156°E in April 2012. Red colors indicate eastward flow, blue westward. Gray lines: contours of potential density (contour interval: 0.2 kg m^{-3}). Black line: mixed layer depth. (b) fQ along isopycnals (see text for definition) averaged between isopycnals with mean depth 100–120 m as a functional of latitude. (c) Same as (b) but averaged between 180 and 200 m. The thin lines in (b) and (c) are $f^2N_0^2$, where N_0^2 is the average N^2 along the layers. (Note, the latitudinal ranges in (b) and (c) are different.).

spectrum for v is higher than that for u in this wavenumber band, particularly at the equator. Similar peaked spectra are shown in Richards et al. (2015) (it should be noted that the spectra in Richards et al. [2015] were multiplied by a spurious factor of 2π). The shear spectra themselves (in a log–log plot) have a steep slope at high wavenumber of ~ -4 suggesting above a wavelength of $\sim$5 m (the shortest resolved scale of the processed LADCP data) there is a clear separation of scales from smaller turbulent motions.

Possible reasons for the presence of the SVSs include wind-driven internal wave activity (Natarov & Richards, 2019) and inertial instability (Natarov & Richards, 2015). With regard the latter, the positioning of both the EUC and NECC is such that the lateral shear is conducive to inertial instability (Natarov & Richards, 2015; Richards & Edwards, 2003). The along isopycnal value of fQ averaged between isopycnals with mean depth 100–120 m and 180–200 m is shown in Figures 1b and 1c, respectively, where f is the Coriolis parameter and Q is the potential vorticity approximated by $(f - \partial u/\partial y)N^2$, that is, assuming $\partial u/\partial y \gg \partial v/\partial x$ and the hydrostatic approximation (Vallis, 2006), with u and v the components of velocity in the zonal and meridional directions (x, y), respectively, and N the buoyancy frequency. For comparison, the thin lines in Figures 1b and 1c are the background $fQ = f^2N_0^2$, where N_0^2 is the average N^2 along the layers. The depth averaged fQ between 180 and 200 m is negative between 0.5°S and 0.4°N, a necessary condition for inertial

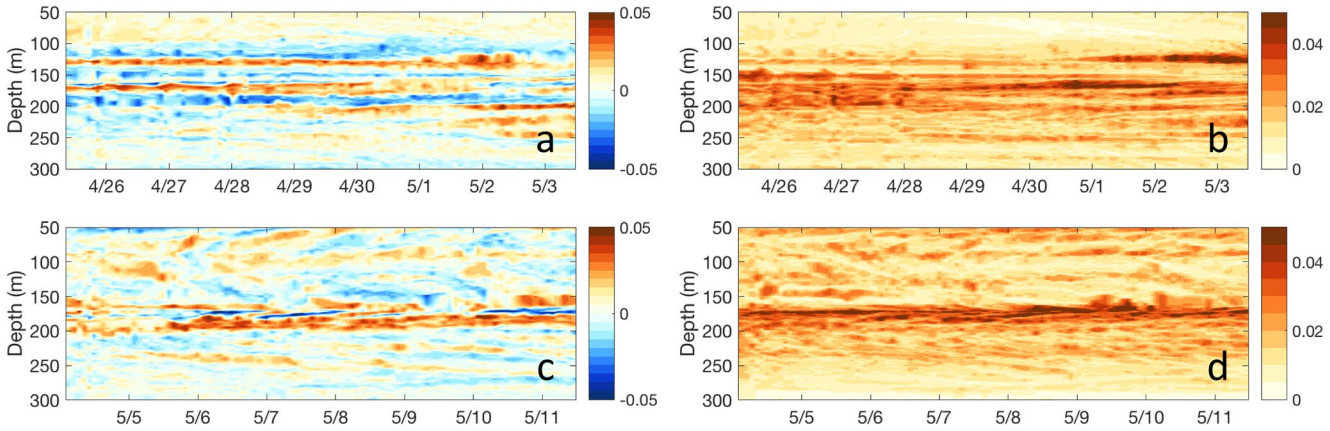

Figure 2. Time series of variables on potential density surfaces at the equator, 156°E plotted as mean depth of the density surface versus time: (a) vertical shear of the meridional component of velocity, $\partial v/\partial z$ (s^{-1}) and (b) Buoyancy frequency, N (s^{-1}). (c, d) As (a) and (b) but for the time series at 1.375°N, 156°E. Time is given as month/day for the year 2012.

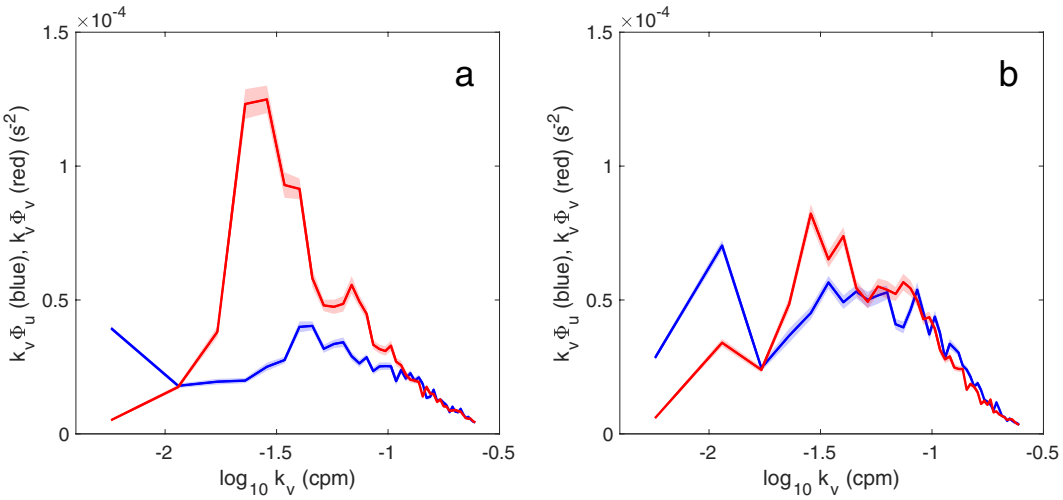

Figure 3. Variance preserving spectra of the zonal and meridional components of shear (blue and red lines, respectively) as a function of the inverse vertical wavelength, k_v: (a) equator, 156°E and (b) 1.375°N, 156°E. Shading shows ±1 standard error based on variation between spectra of individual profiles. The spectra are calculated from profiles between 75 and 250 m depth.

instability, while between 100 and 120 m fQ is close to 0 from the equator to 2°N, consistent with the mature phase of the instability (Natarov & Richards, 2015).

The time mean turbulent kinetic energy dissipation rate, ϵ, from the two time series is shown in Figure 4 (red lines) as a function of depth over the depth range 50–350 m. Both show elevated ϵ between 100 and 250 m, but with different vertical distributions.

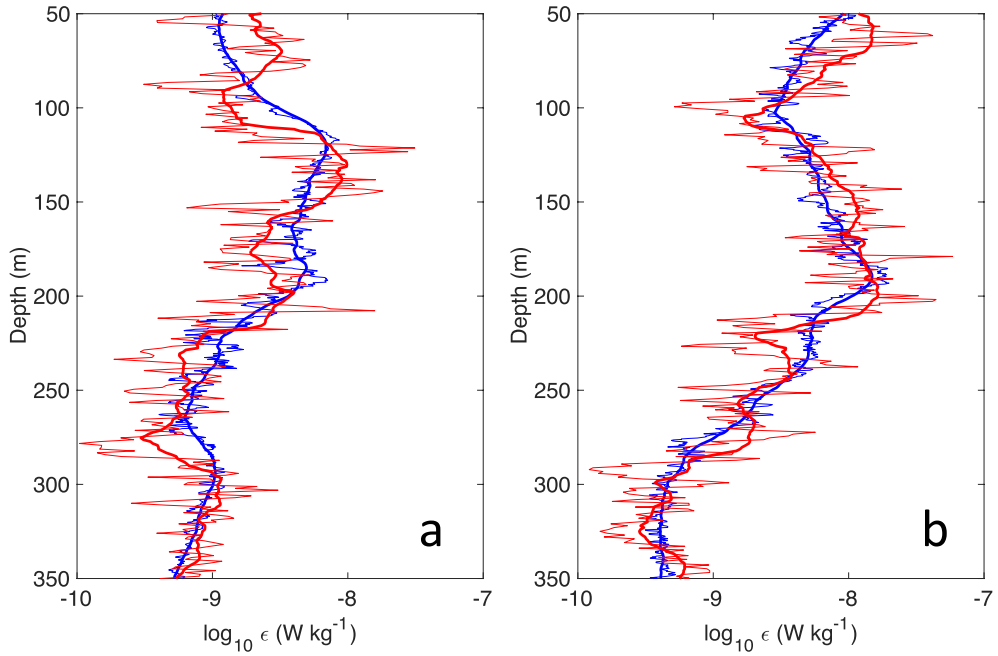

Figure 4. (a) Time mean turbulent kinetic energy dissipation rate, ϵ, for the time series at the equator, as a function of depth (thin lines). Thick lines: with 10 m running averaged applied. Red lines: observed. Blue lines: estimated using 1–3. (b) As (a) but for the time series at 1.375°N.

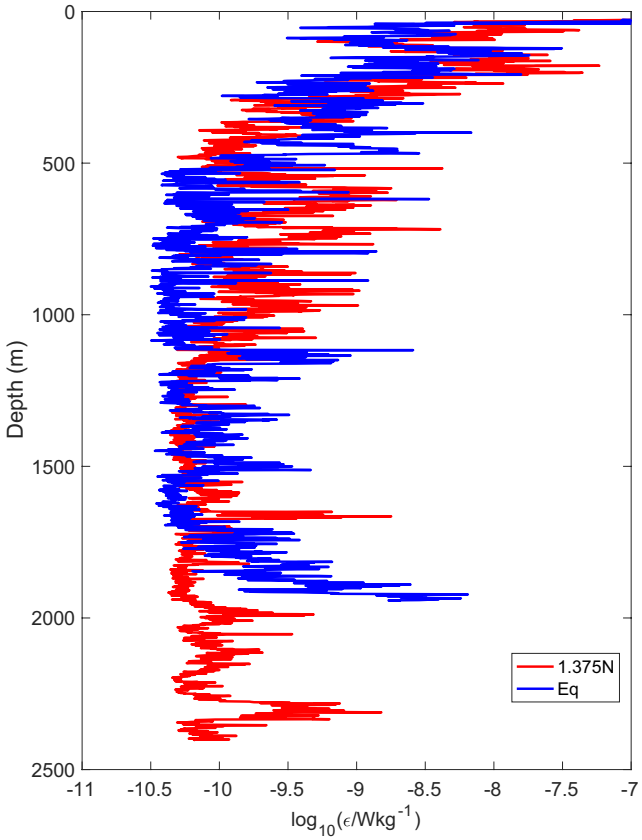

Figure 5. Time mean turbulent kinetic energy dissipation rate, ϵ, over the full depth of profiles for the time series at the equator (blue) and 1.375°N (red).

The full depth range profiles of time mean ϵ are shown in Figure 5. There are patches of elevated mean ϵ below the thermocline at each location, for instance between 500 and 1,000 m depth at 1.375°N and an increase toward the bottom at the equator.

3. Scaling of Shear-Generated Turbulence

We start by writing the turbulent kinetic energy dissipation rate, ϵ, as

$$\epsilon = \ell_v^2 N^3 f(Ri) \tag{1}$$

(see e.g., Richards et al., 2015) where ℓ_v is a turbulent length scale and $f(Ri)$ is a function of the Richardson number, Ri $(=N^2/S^2)$, with $S^2 = (\partial u/\partial z)^2 + (\partial v/\partial z)^2$. An equivalent choice would be $\epsilon = \ell_v^2 S^3 g(Ri)$, where the unknown function $g(Ri) = Ri^{1.5} f(Ri)$. We note that with $f(Ri) = 1$, the length scale ℓ_v is the Ozmidov scale, $L_O = \sqrt{\epsilon / N^3}$ (the vertical scale at which buoyancy forces inhibit vertical motions). With $f(Ri) = Ri^{-3/2}$ then ℓ_v is the Corrsin scale, $L_C = \sqrt{\epsilon / S^3}$ (the scale at which the large-scale shear deforms turbulent eddies).

The length scale ℓ_v can be written as

$$\ell_v = c \frac{u_t}{N}, \tag{2}$$

where u_t is a velocity scale. Taking u_t to be the horizontal velocity scale of the turbulent flow then this scaling for the turbulent length scale, ℓ_v, has been found in a number of studies on stratified turbulent flows when the flow is considered to be in the strong turbulence limit: the strong turbulence limit is when the buoyancy Reynolds number $\mathcal{R} = \epsilon / (\nu N^2) \gg 1$, where ν is the kinematic viscosity of the fluid (e.g., Bartello & Tobias, 2013; Brethouwer et al., 2007; Godeferd & Staquet, 2003; Waite & Bartello, 2004). The measurements used here indicate the turbulence is in the strong regime. We have introduced a nondimensional constant c which will be determined by fitting 1 to observations.

To express u_t in terms of an observable quantity, we assume $u_t \simeq 0.1\tilde{u}$ where $\tilde{u}$ is a measure of the amplitude of the SVS flow features. The factor 0.1 is based on experimental and DNS studies and is expected to be a rough upper bound with substantially smaller values as the turbulence grows and decays (see e.g., Figure 12 of Koop & Browand, 1979; Figures 2 and 3 of Smyth et al., 2005).

Based on measurements from multiple cruises to the western equatorial Pacific, Richards et al. (2015) find $\epsilon \sim N$ at constant Richardson number, which implies $\ell_v \sim 1/N$. They argue that this is equivalent to 2 by noting the depth average value of $\tilde{u}$ (and hence u_t) was approximately constant between the data sets considered.

Here, we will consider $\tilde{u}$ in more detail. In particular, given the differences in the vertical distribution of SVS features in Figure 2, we will consider the vertical distribution of $\tilde{u}$. For each profile of u and v, we apply a wavelet transform (using a Morlet wavelet) and then average the local wavelet power spectrum between 10 and 50 m wavelength. The resulting profiles are normalized so that their depth average between 50 and 250 m is equal to the variance of the original velocity component profile (the variance of the original profile being calculated after a high-pass Fourier filter was applied with a cutoff of 100 m to capture the peak in the shear spectrum). The SVS velocity scale $\tilde{u}$ is then taken as the root mean square of the individual profiles, $\tilde{u}_u$ and $\tilde{u}_v$, from the velocity components u and v, respectively. An example of an individual profile of the meridional component of velocity, v, and associated SVS scale $\tilde{u}_v$, taken from the time series at 1.375°N is shown in Figure 6a. The SVS scale $\tilde{u}_v$ captures the large amplitude SVS activity centered on approximately

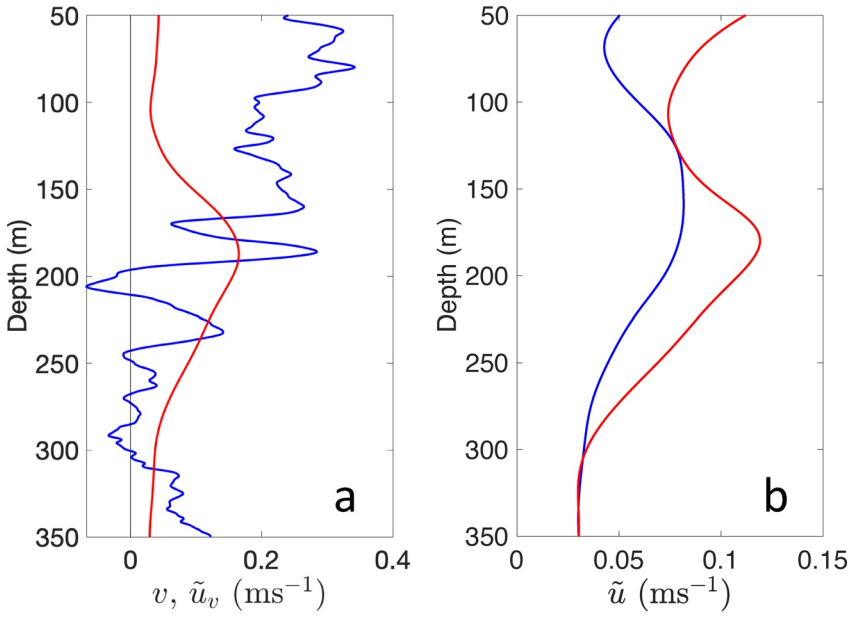

Figure 6. (a) Sample vertical profile from the time series at 1.375°N of v (red line) and $\tilde{u}_v$ (blue line). (b) Time mean of SVS velocity scale, $\tilde{u}$, as a function of depth (see text for definition). Blue line: equatorial time series. Red line: 1.375°N time series.

200 m depth with smaller values above and below. The full SVS velocity scale $\tilde{u}$ $(=(\tilde{u}_u^2 + \tilde{u}_v^2)^{1/2})$ is used in 1 and 2 to estimate ϵ for each profile.

The SVS velocity scale $\tilde{u}$ averaged over each time series is shown in Figure 6b as a function of depth at the equator and 1.375°N. The time mean vertical profiles of $\tilde{u}$ at the two sites are different. At the equator, the mean $\tilde{u}$ is elevated over a relatively broad depth range between 100 and 200 m with a maximum of approximately 0.08 m s^{-1}. In contrast, the profile at 1.375°N is more peaked at a depth of 180 m with a maximum values of 0.12 m s^{-1}. The SVS velocity scale, $\tilde{u}$ drops off with depth for both time series to a value of approximately 0.03 m s^{-1} at 350 m depth.

Lastly, $f(Ri)$ needs to be specified. We will take

$$f(Ri) = e^{-bRi} \tag{3}$$

for $Ri < 0.25$. Fitting 1 to the distribution found by Richards et al. (2015) (their Figure 6), we obtain $b = 4.81$. For $Ri > 0.25$, f is ramped down to 0 at $Ri = 0.5$ and remains 0 for higher values of Ri. Note that there is only a modest increase in f as Ri tends to 0; $f(Ri)$ increases only by a factor of 3 from $Ri = 0.25$ to $Ri = 0$. This is in contrast to some other formulations such as that of Kunze et al. (1990) (see Figure 6, Richards et al., 2015). We will discuss the sensitivity to our choices in the next section but note here that the vertical distribution of ϵ as prescribed by 1 is much more dependent on the vertical distribution of ℓ_v through variations in $\tilde{u}$ than the functional form of f.

4. Comparison With Observations

The scaling described above involves relating the turbulent kinetic energy dissipation rate, ϵ, to the turbulent length scale, ℓ_v, the buoyancy frequency, N, and a function of the Richardson number $f(Ri)$: Equations 1–3. In addition, we relate the turbulent velocity scale, u_t, to the SVS velocity scale $\tilde{u}$, by $u_t = 0.1\tilde{u}$.

To evaluate the scheme, we utilize the two time series at the equator and 1.375°N each of which have around 90 vertical profiles of velocity and density. The vertical shear, S, has a nominal vertical resolution of 2 m, while N is calculated from 1 decibar (~1 m) averages of salinity and temperature. The analysis of Richards et al. (2015) suggests that this resolution is more than adequate in capturing the relevant shear

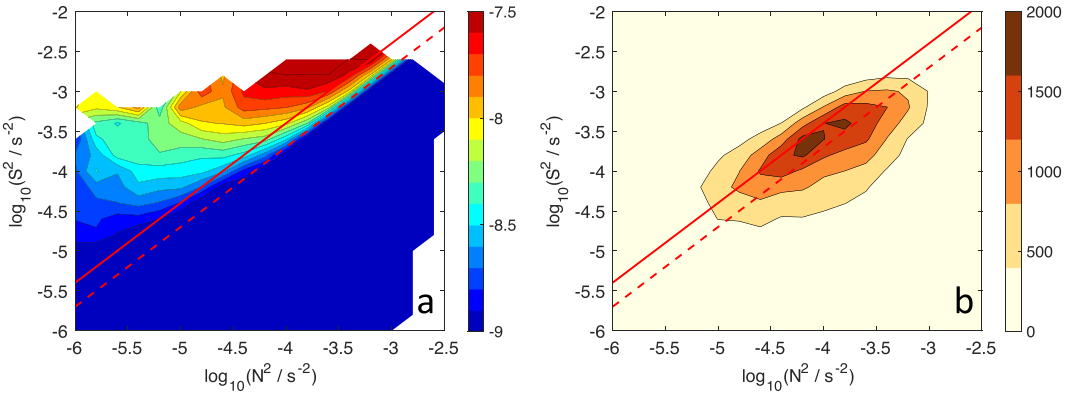

Figure 7. (a) Turbulent kinetic energy dissipation rate, ϵ, estimated from 1, bin averaged with respect to $\log_{10} S^2$ and $\log_{10} N^2$, for the equatorial time series for data between depths 50 and 250 m. (b) Number of occurrences in each bin average. Solid red line $Ri = 0.25$. Dashed red line $Ri = 0.5$.

and stratification. Data are interpolated onto a common 1 m vertical grid and ϵ calculated using 1. The SVS velocity scale, $\tilde{u}$, is calculated for each profile as outlined above. The resultant estimate for ϵ is then averaged over all profiles for each time series. The result is shown in Figure 4 for each time series (blue lines) and compared to the observed averaged profiles (red lines).

The constant c in 2 is taken to be $c = 0.24$, which is the mean value of c for each time series got by fitting the estimated ϵ to the observed over the depth interval 100–250 m (c estimated in this way for each time series is 0.23 ± 0.02 and 0.25 ± 0.02, respectively). Given that our use of $u_t = 0.1\tilde{u}$ is an upper bound on u_t, the value of c (and its small variation between time series) suggests the scalings used are appropriate.

The estimated ϵ compares remarkably well for both time series over the depth interval 50–350 m. In particular, the change in vertical distribution and amplitude are captured well. It is stressed that much of the vertical variation in the estimated ϵ is controlled by the vertical variation in the estimated vertical scale ℓ_v through the assumed dependence on $\tilde{u}$ (compare Figure 4 with Figure 6: see also Figures 9 and 10). The SVS velocity scale, $\tilde{u}$, is only modestly sensitive to our choices in how $\tilde{u}$ is computed. For instance, the 50 m cutoff for the wavelet spectrum was chosen to limit end effects (the cone-of-influence). Increasing this to 100 m gives a slightly degraded (visual) fit over the full depth, with the fitted value of c increased slightly by 5%. Similarly, decreasing the low cutoff from 10 to 5 m results in a decrease in the fitted c of 5%.

The turbulent kinetic energy dissipation rate, ϵ, estimated from 1, bin averaged with respect to $\log_{10} S^2$ and $\log_{10} N^2$, together with the number of occurrences in each bin average, is shown in Figure 7 for the equatorial time series for data between depths 50 and 250 m. The distributions are very similar to those shown in Figures 4a and 4b. Richards et al. (2015) showing an increase in ϵ at constant Richardson number for increasing N^2 (equivalently, increasing S^2) and the peak in the number of occurrences between $Ri = 0.25$ and 0.5.

The vertical variation of the time mean of the turbulent length scale, ℓ_v, given by 2 is shown in Figure 8 for the two time series. At the equator, overall there is a slight decrease of ℓ_v with depth to a value of approximately 0.2 m at 300 m depth followed by an increase. At 1.375°N, between 50 and 150 m, ℓ_v is somewhat larger than at the equator with a value around 0.4 m. There is a sharp decrease at 150 m with ℓ_v reducing to around 0.2 m. Again, there is an increase in ℓ_v at deeper depths, in this case starting around 250 m depth.

The time mean turbulent length scale, ℓ_v, is compared to the time mean Ozmidov scale $\ell_o = \sqrt{\epsilon / N^3}$ in Figure 8. The vertical variation of the two length scales is similar in both time series. Between 175 and 275 m, they are very similar in magnitude. Between 50 and 150 m, ℓ_o is greater than ℓ_v by a factor of approximately 1.5 on average in both cases. It should be noted that ℓ_v equals ℓ_o when $f(Ri) = 1$ (Equation 1). Differences between the two therefore reflect to a certain degree the impact of variations in the contribution coming from $f(Ri)$. This is not exact, however, as the observed ϵ is used to calculate ℓ_o, and there are differences in the observed and estimated ϵ (Figure 4) (and we are comparing the averages of the product of different variables). The influence of $f(Ri)$ on the vertical distribution of ϵ is better seen in Figures 9c and 10c.

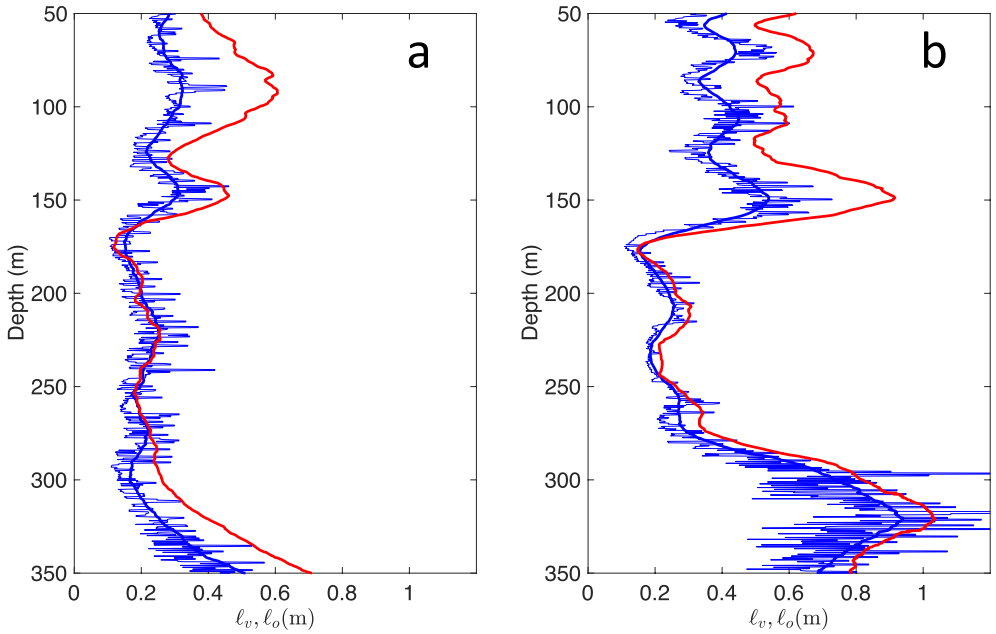

Figure 8. (a) Time mean of the turbulent length scale ℓ_v against depth (blue thin line), with a 10 m running averaged applied (thick blue line) and the time mean of the Ozmidov length scale ℓ_o with a 10 m running averaged applied (thick red line), for the equatorial time series. (b) As (a) but for the 1.375°N time series.

5. Deconstruction of the Scaling

Combining 1 and 2, and relating the turbulent velocity scale u_t to the SVS velocity scale $\tilde{u}$, gives

$$\epsilon \sim \tilde{u}^2 N f(Ri). \tag{4}$$

To determine which factor most influences the vertical distribution of ϵ, we plot the time mean of each term on the right-hand side of 4 separately in Figures 9 and 10a–10c for the equatorial and 1.375°N time series, respectively. Each term has been normalized with its depth mean to emphasize the depth variation. The fourth panel (d) in each figure shows the time mean of ϵ estimated from 4. Here, ϵ has been normalized with its value averaged between 250 and 300 m depth. Also shown in panel (d) is the product of the time mean of the three terms on the right-hand side of 4, normalized in the same way (thin dashed blue line), which captures much of the vertical variation of the time mean of ϵ.

Also shown in Figures 9d and 10d is ϵ estimated by 4 but with $\tilde{u}$ held constant (i.e., $\epsilon \sim Nf(Ri)$: red line in the figures). Again the estimate of ϵ has been normalized by its value averaged between 250 and 300 m. The vertical variation in ϵ is reduced substantially at both locations compared with when the full expression 4 is used. Much of the vertical variation in N is compensated by the variation in $f(Ri)$. The vertical variation in ϵ is very much reflected in the variations in $\tilde{u}^2$; compare Figures 9a and 9d, and Figures 10a and 10d.

To test the sensitivity to the choice of $f(Ri)$, in Figures 9c and 10c, we compare the time mean normalized vertical variation of our choice of $f(Ri)$ with the functional form, $f_k(Ri)$, suggested by Kunze et al. (1990). Their expression for ϵ can be written $\epsilon_k \sim \Delta z N^3 f_k(Ri)$, where Δz is the thickness of a layer where $Ri < Ri_{cr}$ and Ri_{cr} is critical Richardson number taken here to be 0.5 to be consistent with our choice of when $f(Ri)$ becomes 0 (Equation 6 of Richards et al. [2015]). The vertical variation of the time mean $f(Ri)$ and $f_k(Ri)$ is very similar at both locations despite their very different behavior at small Ri ($f_k(Ri) \sim 1/Ri^{3/2}$ for $Ri \ll Ri_{cr}$). The reason for this similarity is the distribution of data in (N^2, S^2) space is confined and centered on Ri between 0.25 and 0.5 (Figure 7b). (Note, the scaling ϵ_k is similar to 4 if $\Delta z \sim \tilde{u} / N$ which is explored by Richards et al. [2015].)

Referring back to Section 4 and the Ozmidov scale, the vertical variation in $f(Ri)$ in Figure 9c is similar to the vertical variation of the difference between ℓ_o and ℓ_v in Figure 8a, that is, $\ell_o > \ell_v$ where $f(Ri)$ is larger. It

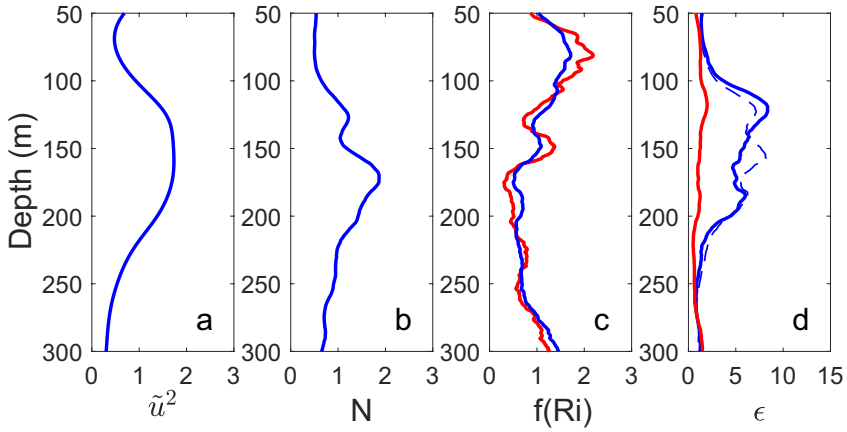

Figure 9. Normalized time mean of quantities from the equatorial time series. (a) $\tilde{u}^2$, (b) N, and (c) $f(Ri)$, normalized with their depth averages over the depth interval 50–300 m. (d) Estimated turbulent kinetic energy dissipation rate, ϵ, normalized with its value averaged between 250 and 300 m. In (c): blue line $f(Ri)$ using 3, red line using $f_k(Ri)$ from Kunze et al. (1990). In (d): blue line, ϵ estimated from 4; red line, ϵ estimated from $Nf(Ri)$; dashed blue line, product of the time mean of quantities on the RHS of 4.

is less so comparing Figures 10c and 8b, although we note the values above 150 m are elevated in both ℓ_o/ℓ_v and $f(Ri)$ compared with slightly deeper values. An increase in $f(Ri)$ is given by a decrease in Ri. This is consistent therefore with the observation that the Thorpe scale tends to be smaller than the Ozmidov scale when Ri is small (see e.g., Dillon, 1982). (Note, that because of the smallness of the length scales, we are unable to calculate the Thorpe scale from the CTD data, and we did not have a high frequency salinity probe on the VMP.)

6. Vertical Distribution of the Vertical Diffusion Coefficient

Combining 1 and 2, the vertical turbulent diffusion coefficient, κ_v $(= \gamma\epsilon/N^2)$ (Osborn, 1980) becomes

$$\kappa_v = \frac{c\gamma u_t^2 f(Ri)}{N}, \tag{5}$$

where we take $u_t = 0.1\tilde{u}$ and $c = 0.24$. We will take the mixing efficiency $\gamma = 0.2$, recognizing the uncertainties in the value of γ and expected spatial and temporal variations. Ijichi and Hibiya (2018) find a tendency

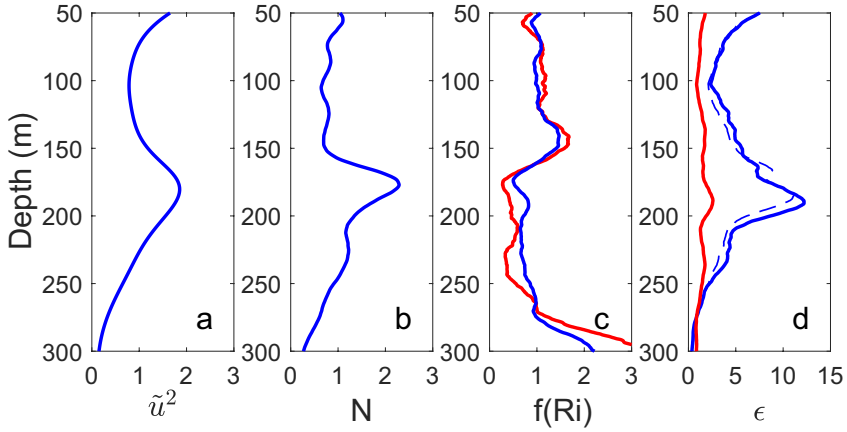

Figure 10. Same as Figure 9 except from the time series at 1.375°N.

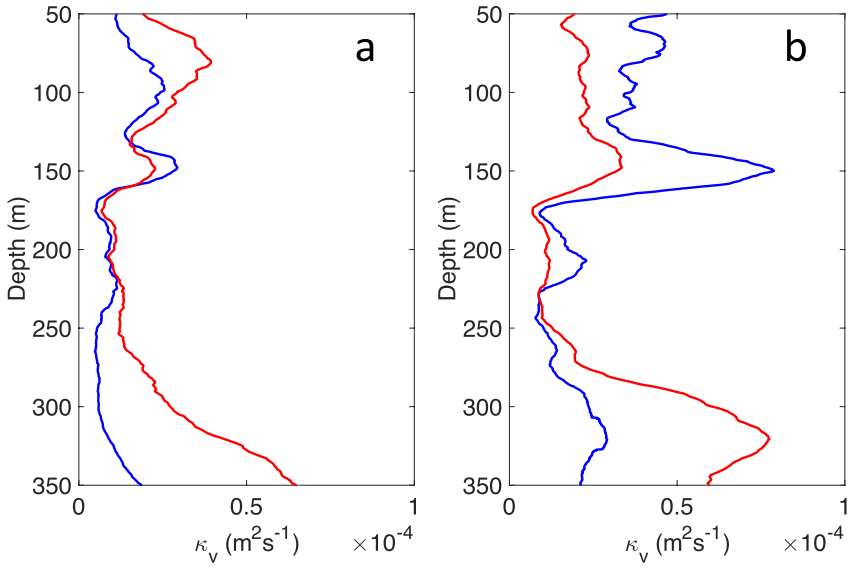

Figure 11. (a) Time mean vertical diffusion coefficient, κ_v. (a) At the equator. (b) At 1.375°N. Blue line: estimated by 5. Red line: KPP estimate 6 with $\kappa_o = 1.8 \times 10^{-4}$ m^2 s^{-1} and $Ri_{cr} = 0.3$. A 10 m running mean has been applied to each profile.

for γ to increase with depth as the stratification weakens, but in depths less than 500 m the spread of values of γ is approximately centered on 0.2. Here, we are interested in how the scaling of ϵ given in 4 translates to κ_v.

The time mean κ_v estimated by 5 is shown in Figures 11a and 11b (blue lines) for the equator and 1.375°N time series, respectively. The factor N^{-2} reshapes the vertical profile of κ_v compared to ϵ (see Figures 9d and 10d, respectively) such that κ_v is reduced in the pycnocline at around 200 m depth for the 1.375°N time series where $\tilde{u}$ and ϵ peak, and the maximum value of κ_v occurs at a somewhat shallower depth. The depth averaged κ_v between 50 and 170 m for the 1.375°N time series (4.6×10^{-5} m^2 s^{-1}) is more than twice that at the equator (2.0×10^{-5} m^2 s^{-1}). Below the pycnocline, the reduced SVS activity (reduced $\tilde{u}$) tends to compensate the reduced stratification such that we do not see a marked increase in κ_v.

The vertical variation in κ_v is dependent on the combination of the vertical variations of Ri, $\tilde{u}$ and N. To compare with a scheme that considers only the first of these, the Richardson number, in Figures 11a and 11b (red lines), we show the results using the KPP scheme of Large et al. (1994) for shear-generated turbulence, namely

$$\kappa_{KPP} = \kappa_o \left(1 - \left(\frac{Ri}{Ri_{cr}}\right)^2\right)^3 \tag{6}$$

for $Ri < Ri_{cr}$. We have chosen $\kappa_o = 1.8 \times 10^{-4}$ m^2 s^{-1} and $Ri_{cr} = 0.3$, which gives a reasonable fit to data collected in the western equatorial Pacific (cf., Richards et al., 2015). Both these values are well below those suggested by Large et al. (1994) (namely 50×10^{-4} m^2 s^{-1} and 0.7, respectively). (A value of $Ri_{cr} = 0.3$ gives a better fit to the data than $Ri_{cr} = 0.25$ shown in Figure 8 of Richards et al. [2015], for values of Ri around 0.25.) The results are somewhat sensitive to the choice of Ri_{cr}. For instance, the mean value between 150 and 250 m is reduced by approximately 25% with $Ri_{cr} = 0.25$ but increased by more than a factor of 3 for $Ri_{cr} = 0.7$, for both time series. (Employing the value of κ_o suggested by Large et al. [1994] increases κ_{KPP} by a factor close to 30.)

Despite the large vertical variations in $\tilde{u}$ and N, there are qualitative similarities between the profiles of κ_v and κ_{KPP}. There are, however, important quantitative differences. For instance, above 125 m depth, there is an increase in κ_v at 1.375°N compared with the equator. With κ_{KPP}, there is a decrease between the two. κ_{KPP} captures the local maximum in κ_v centered on 150 m at both sites but is smaller in magnitude and does not

display the large increase at 1.375°N. Below 250 m, κ_{KPP} diverges from κ_v. As stated above, for κ_v, given by 5, the reduction with depth in $\tilde{u}$ below the thermocline (see Figures 9a and 10a) partially compensates for the reduction in N. For KPP, with a constant κ_o, there is no compensation and the KPP estimate at 350 m is approximately 3 times that given by 5 at both sites.

7. Discussion

We have presented a framework to study shear-generated turbulence and its scaling. We have couched the problem in terms of quantities in the ocean or atmosphere that, depending on the situation, may be measurable or resolved in models. A major assumption is that the Richardson number is an important parameter in determining whether or not there is turbulent activity. A key aspect, however, is to shift emphasis away from the functional form of the Richardson number to consideration of the time and length scales controlling the turbulent activity. In particular, we assume a scaling for the vertical length scale of the turbulent flow found from theoretical considerations, DNS studies, and previous measurements in the western equatorial Pacific.

To test our proposed scaling, we have compared it to observations of the turbulent kinetic energy dissipation rate, ϵ, taken in the western equatorial Pacific. The time-averaged ϵ estimated by the scaling given by 1 using the data from time series compares well with the observed average. The estimated ϵ captures the differences in observed vertical structure and amplitude of the two time series. Much of the vertical variation of ϵ is found to be controlled by the vertical variation in velocity scale, $\tilde{u}$, of the fine-scale (SVS) velocity variations.

When making direct comparisons of flow features, such as the vertical shear and turbulence activity, it is important that appropriate flow structures are resolved. In this regard, the western equatorial Pacific is an ideal location to study shear-generated turbulence. The vertical shear responsible for much of the turbulent activity often has a distinct vertical scale that is resolvable using appropriate instrumentation (Richards et al., 2015).

Of course, being able to resolve, the relevant shear is not always the case and the direct application of 1 will be limited. For instance, spectral transfers in the internal gravity wave field increase energy at high vertical wavenumbers and the spectral characteristics of the unresolved shear need to be taken into account (see e.g., Gregg, 1989; Kunze, 2017, and related studies). In contrast, the shear associated with near-inertial waves is often resolvable, with their shear contributing to mixing (see e.g., Alford et al., 2016) and 1, may well be applicable.

An aspect that warrants further investigation is the turbulent velocity scale u_t. Here, we have assumed u_t is related to the velocity scale of the flow features that dominate the vertical shear, $\tilde{u}$. We average over a number of turbulent events at various times in their evolution during the ~7-day time series. Based on DNS studies, this is a not an unreasonable assumption (cf., Smyth et al., 2005), although those studies show the relationship to vary as a turbulent event evolves. There may be differences, therefore, in a time-averaged sense for different flow regimes and appropriate DNS studies, as well as observations in different regimes, are required to determine those differences (and including more direct observational estimates of u_t, e.g., Beaird et al., 2012; Moum, 1990; Thurnherr et al., 2015). In the present study, the shear during the equatorial time series was persistent in time (Figure 2a) and in part likely induced by inertial instability. Wind-generated inertia gravity waves can produce event-like mixing events (e.g., Soares et al., 2016) which may have different time-averaged characteristics. We note, however, the shear at 1.375°N is less temporally coherent than at the equator, apart from along the pycnocline (Figure 2c). Despite these differences, our scaling for u_t appears to work well for both time series.

With regard to $\tilde{u}$, we use a wavelet transform to determine its vertical distribution, giving a fairly large vertical scale to its variation with depth (see Figure 6a). There is, therefore, a difference in the vertical scale of the our estimated $\tilde{u}$ and N, the latter got from 1 m averages of CTD data. In the case considered here, this does not appear to be too much of an issue. Using the time averaged, and therefore much smoother, N gives a time-averaged estimate of ϵ that is not too different from using individual profiles of N (see Figures 9 and 10). Further consideration may be needed in how $\tilde{u}$ is estimated, particularly if 1 is used as a parameterization. In particular, in cases where there are isolated shear layers, it may be more appropriate to use a more local measure of the velocity difference across each layer.

We find the vertical distribution of the estimated vertical diffusion coefficient is dependent on the vertical variations of Ri, $\tilde{u}$, and N. Indeed, if the variations in the latter two are ignored, such as in KPP, there are substantial differences in the vertical distribution (see Figure 11). But how important is the vertical variation in the vertical diffusion coefficient? This needs to be ascertained for particular flows. Sasaki et al. (2013) find it to be important for large-scale ocean–atmosphere interactions in the tropical Pacific. In a related study, Jia et al. (2021) find with enough vertical resolution in a model of the tropical Pacific (enough to start to resolve the observed fine-scale structures in the vertical shear) the associated vertical distribution of the eddy diffusivity (derived using KPP) changes the structure of the equatorial thermocline, which in turn impacts the temperature in the equatorial Pacific cold tongue. It remains to be seen how large an impact the differences seen in Figure 11 have.

Data Availability Statement

Data used in this study were collected on cruise KM1208 of the R/V Kilo Moana and can be found at the R2R data archive at https://www.rvdata.us/search/vessel/km1208 with microstructure data at https://microstructure.ucsd.edu/. Processed CTD, LADCP, and microstructure data can be found at ftp://ftp.soest.hawaii.edu/kelvin/MIXET.

Acknowledgments
We are particularly thankful to Captain Dewry and crew of the R/V Kilo Moana and the UH OTG for their expertise and enthusiastic help in collecting the data. This work was supported by the U.S. National Science Foundation under grant NSF OCE-1029722 and the U.S. National Oceanic and Atmospheric Administration under grant NA18OAR4310404. K.J.R. also acknowledges support from the Kavli Institute of Theoretical Physics and the National Science Foundation under grant NSF PHY-1748958. We would like to thank Ilker Fer and an anonymous reviewer whose thoughtful comments led to improvements of the manuscript.

References

Alford, M. H., MacKinnon, J. A., Simmons, H. L., & Nash, J. D. (2016). Near-inertial internal gravity waves in the ocean. *Annual Review of Marine Science*, *8*, 95–123.

Bartello, P., & Tobias, S. M. (2013). Sensitivity of stratified turbulence to the buoyancy Reynolds number. *Journal of Fluid Mechanics*, *725*, 1–22.

Beaird, N., Fer, I., Rhines, P., & Eriksen, C. (2012). Dissipation of turbulent kinetic energy inferred from seagliders: An application to the eastern Nordic Seas overflows. *Journal of Physical Oceanography*, *42*, 2268–2282.

Brethouwer, G., Billant, P., Lindborg, E., & Chomaz, J.-M. (2007). Scaling analysis and simulation of strongly stratified turbulent flows. *Journal of Fluid Mechanics*, *585*, 343–368.

Dillon, T. M. (1982). Vertical overturns: A comparison of Thorpe and Ozmidov length scales. *Journal of Geophysical Research*, *87*, 9601–9613.

Godeferd, F. S., & Staquet, C. (2003). Statistical modelling and direct numerical simulations of decaying stably stratified turbulence. Part 2. Large-scale and small-scale anisotropy. *Journal of Fluid Mechanics*, *486*, 115–159.

Goodman, L., Levine, E. R., & Lueck, R. G. (2006). On measuring the terms of the turbulent kinetic energy budget from an AUV. *Journal of Atmospheric and Oceanic Technology*, *23*, 977–990.

Gregg, M. C. (1989). Scaling turbulent dissipation in the thermocline. *Journal of Geophysical Research*, *94*, 9686–9698.

Ijichi, T., & Hibiya, T. (2018). Observed variations in turbulent mixing efficiency in the deep ocean. *Journal of Physical Oceanography*, *48*(8), 1815–1830.

Jia, Y., Richards, K. J., & Annamalai, H. (2021). The impact of vertical resolution in reducing biases in sea surface temperature in a tropical Pacific Ocean model. *Ocean Modelling*, *157*, 101722. https://doi.org/10.1016/j.ocemod.2020.101722

Koop, C. G., & Browand, F. K. (1979). Instability and turbulence in a stratified fluid with shear. *Journal of Fluid Mechanics*, *93*, 135–159.

Kunze, E. (2017). Internal-wave-driven mixing: Global geography and budgets. *Journal of Physical Oceanography*, *47*, 1325–1345.

Kunze, E., Williams, A. J., III, & Briscoe, M. G. (1990). Observations of shear and vertical stability from a neutrally buoyant float. *Journal of Geophysical Research*, *95*, 18127–18142.

Large, W. G., McWilliams, J. C., & Doney, S. C. (1994). Oceanic vertical mixing: A review and a model with a nonlocal boundary layer parameterization. *Reviews of Geophysics*, *32*, 363–403.

Moum, J. N. (1990). Profiler measurements of vertical velocity fluctuations in the ocean. *Journal of Atmospheric and Oceanic Technology*, *7*, 323–333.

Natarov, A., & Richards, K. J. (2015). Persistent presence of small vertical scale velocity features during three-dimensional equilibration of equatorial inertial instability. *Physics of Fluids*, *27*, 084109.

Natarov, A., & Richards, K. J. (2019). Enhanced energy dissipation in the equatorial pycnocline by wind-induced internal wave activity. *Journal of Geophysical Research: Oceans*, *124*, 6200–6217. https://doi.org/10.1029/2019JC015228

Osborn, T. R. (1980). Estimates of the local rate of vertical diffusion from dissipation measurements. *Journal of Physical Oceanography*, *10*, 83–89.

Pacanowski, R. C., & Philander, S. G. H. (1981). Parameterization of vertical mixing in numerical models of tropical oceans. *Journal of Physical Oceanography*, *11*, 1443–1451.

Peters, H., Gregg, M. C., & Toole, J. M. (1988). On the parameterization of equatorial turbulence. *Journal of Geophysical Research*, *93*, 1199–1218.

Richards, K. J., & Edwards, N. R. (2003). Lateral mixing in the equatorial Pacific: The importance of inertial instability. *Geophysical Research Letters*, *30*(17), 1888. https://doi.org/10.1029/2003GL017768

Richards, K. J., Natarov, A., Firing, E., Kashino, Y., Soares, S. M., Ishizu, M., et al. (2015). Shear-generated turbulence in the equatorial Pacific produced by small vertical scale flow features. *Journal of Geophysical Research: Oceans*, *120*, 3777–3791. https://doi.org/10.1002/2014JC010673

Sasaki, W., Richards, K. J., & Luo, J.-J. (2013). Impact of vertical mixing induced by small vertical scale structures above and within the equatorial thermocline on the tropical Pacific in a CGCM. *Climate Dynamics*, *41*(2), 443–453. https://doi.org/10.1007/s00382-012-1593-8

Smyth, W. D., Nash, J. D., & Moum, J. N. (2005). Differential diffusion in breaking Kelvin–Helmholtz billows. *Journal of Physical Oceanography*, *35*, 1004–1022.

Soares, S. M., Natarov, A., & Richards, K. J. (2016). Internal swells in the tropics: Near-inertial wave energy fluxes and dissipation during CINDY. *Journal of Geophysical Research: Oceans*, *121*, 3297–3324. https://doi.org/10.1002/2015JC011600

Thurnherr, A. M., Kunze, E., Toole, J. M., St Laurent, L., Richards, K. J., & Ruiz-Angulo, A. (2015). Vertical kinetic energy and turbulent dissipation in the ocean. *Geophysical Research Letters*, *42*, 7639–7647. https://doi.org/10.1002/2015GL065043

Vallis, G. K. (2006). *Atmospheric and oceanic fluid dynamics: Fundamentals and Large-scale Circulation* (745 pp.). Cambridge, UK: Cambridge University Press.

Waite, M. L., & Bartello, P. (2004). Stratified turbulence dominated by vortical motion. *Journal of Fluid Mechanics*, *517*, 281–308.

Zaron, E. D., & Moum, J. N. (2009). A new look at Richardson number mixing schemes for equatorial ocean modeling. *Journal of Physical Oceanography*, *39*, 2652–2664.